



Published in final edited form as:

Biomaterials. 2015 October ; 67: 286–296. doi:10.1016/j.biomaterials.2015.07.016.

Biodegradable, Phosphate-containing, Dual-Gelling Macromers for Cellular Delivery in Bone Tissue Engineering

Brendan M. Watson¹, Tiffany N. Vo¹, Alexander M. Tatar¹, Sarita R. Shah¹, David W. Scott², Paul S. Engel³, and Antonios G. Mikos^{1,*}

¹Department of Bioengineering, Rice University, Houston, TX 77030, USA

²Department of Statistics, Rice University, Houston, TX 77251, USA

³Department of Chemistry, Rice University, Houston, TX 77251, USA

Abstract

Injectable, biodegradable, dual-gelling macromer solutions were used to encapsulate mesenchymal stem cells (MSCs) within stable hydrogels when elevated to physiologic temperature. Pendant phosphate groups were incorporated in the N-isopropyl acrylamide-based macromers to improve biointegration and facilitate hydrogel degradation. The MSCs were shown to survive the encapsulation process, and live cells were detected within the hydrogels for up to 28 days *in vitro*. Cell-laden hydrogels were shown to undergo significant mineralization in osteogenic medium. Cell-laden and acellular hydrogels were implanted into a critical-size rat cranial defect for 4 and 12 weeks. Both cell-laden and acellular hydrogels were shown to degrade *in vivo* and help to facilitate bone growth into the defect. Improved bone bridging of the defect was seen with the incorporation of cells, as well as with higher phosphate content of the macromer. Furthermore, direct bone-to-hydrogel contact was observed in the majority of implants, which is not commonly seen in this model. The ability of these macromers to deliver stem cells while forming *in situ* and subsequently degrade while facilitating bone ingrowth into the defect makes this class of macromers a promising material for craniofacial bone tissue engineering.

Keywords

hydrogel; poly(N-isopropyl acrylamide); monoacryloxyethyl phosphate; rat cranial defect; mesenchymal stem cell encapsulation

1.1. Introduction

Tissue engineering generally involves the use of biomaterials, cells, and bioactive factors in various synergistic combinations to facilitate the regeneration of lost or injured tissue. There is a large clinical need for bone tissue engineering strategies to repair damage from

*Corresponding Author: Antonios G. Mikos, Department of Bioengineering, Rice University, 6500 Main Street, Houston, Texas 77030, USA, Tel: 713-348-5355, Fax: 713-348-4244, mikos@rice.edu.

Publisher's Disclaimer: This is a PDF file of an unedited manuscript that has been accepted for publication. As a service to our customers we are providing this early version of the manuscript. The manuscript will undergo copyediting, typesetting, and review of the resulting proof before it is published in its final form. Please note that during the production process errors may be discovered which could affect the content, and all legal disclaimers that apply to the journal pertain.

craniofacial bone trauma as well as congenital abnormalities. Current strategies for craniofacial bone repair use autologous grafts which can be difficult to shape to appropriately match the contours of the face and result in donor site morbidity.[1] Craniofacial bone tissue engineering holds the potential not only to treat without any associated donor site morbidity, but also to reproduce the precise facial contours necessary for aesthetic repair of the damaged region. Injectable materials can be used to deliver stem cells and form *in situ* to match the margins of craniofacial defects and be shaped to match facial contours more easily than autologous grafts, providing a foundation to guide tissue formation.[2] Consequently, injectable, *in situ*-forming materials are promising candidates for craniofacial bone tissue engineering strategies.

Although hydrogels do not possess the mechanical strength necessary to provide support for load-bearing functions, they can be used to fill critical-size bone defects in non-load-bearing areas. Hydrogels are appealing for use in these bony defects because they can be formed *in situ* in a minimally-invasive manner, allowing them to fill a wide variety of defect shapes and sizes. Because of their large aqueous component, hydrogels can be used to deliver and support cells that can improve tissue regeneration.[3, 4] Mesenchymal stem cells (MSCs) are popular cell sources in many bone tissue engineering strategies as they possess a higher proliferative capacity and are often more readily available than mature osteoblastic cells.[5] Thermogelling polymers are appealing for bioengineering applications due to their ability to form rapidly *in situ*. However, their use in cell-delivery applications has been limited because the formed hydrogels undergo post-gelation syneresis (liquid expulsion from the hydrogel), which can adversely affect the viability of encapsulated cells.[6]

Previous work developed and characterized biodegradable methacrylated thermogelling macromers (MA-TGMs)[7] that chemically cross-link after thermogelation to stabilize the hydrogel and mitigate syneresis. These macromers are made from a statistical copolymer of N-isopropyl acrylamide (NiPAAm), acrylamide (AAm), and mono-acryloxyethyl phosphate (MAEP) that are esterified with glycidyl methacrylate (GMA) after polymerization to yield dual-gelling macromers. These macromers are particularly promising for cell-delivery applications, as they degrade via hydrolysis of phosphate ester bonds of MAEP, allowing the macromer backbone to return to solution. Hydrolysis of these phosphate ester bonds is accelerated in the presence of the naturally occurring enzyme alkaline phosphatase, which is upregulated in areas of regenerating bone tissue. Hydrogels that readily undergo enzymatic degradation have demonstrated improved bone growth and infiltration into hydrogels.[8] Incorporation of phosphate groups such as those in MAEP into scaffolds has also been shown to improve biomineralization and biocompatibility in regenerative medicine applications.[9]

Two formulations (high and low MAEP content) of these dual-gelling macromers were selected for *in vitro* and *in vivo* characterization to evaluate their osteogenic potential. The objective of the *in vitro* study was to evaluate the macromer solutions described previously for their ability to encapsulate rat MSCs and characterize cell viability, osteogenic differentiation, and mineralization under osteogenic conditions. The objective of the *in vivo* study was to evaluate the MSC-laden and acellular hydrogels synthesized from macromer solutions for their ability to induce bone growth into and across a critical-size rat cranial

defect. We hypothesized that the encapsulation of MSCs within the hydrogels would accelerate mineralization and help facilitate bony integration. Furthermore, we hypothesized that phosphate groups present in MAEP would improve bony integration and bone regeneration, and that degradation of phosphate ester bonds would help facilitate infiltration of bone tissue.

1.2. Methods

1.2.1. Materials

NiPAAm, AAm, azobisisobutyronitrile (AIBN), GMA, dimethyl sulfoxide (DMSO), D₂O with 0.75 wt% 3-(trimethylsilyl)propionic-2,2,3,3-d₄ acid, sodium salt (TMP), sodium phosphate dibasic, butylated hydroxytoluene, ammonium persulfate (APS), tetramethylethylenediamine (TEMED), acetic acid, β -glycerol 2-phosphate, dexamethasone, ampicillin, amphotericin, gentamicin, silver nitrate, sodium thiosulfate, were purchased from Sigma-Aldrich (St. Louis, MO) and used as received unless otherwise noted. MAEP was purchased from Polysciences Inc. (Warrington, PA). Diethyl ether, acetone (analytical grade), 10% neutral buffered formalin, ethanol (200 proof), Histo-Prep freezing media, and the Quant-iT Picogreen dsDNA Assay kit were obtained from VWR (Radnor, PA). Phosphate-buffered saline (PBS) solution was made from powder (pH 7.4, Gibco Life, Grand Island, NY), and ultrapure water was obtained from a Millipore Super-Q water system (Millipore, Billerica, MA). Complete osteogenic medium (COM) was made from minimal essential medium α (α MEM) (Gibco Life, Grand Island, NY) supplemented with 10% fetal bovine serum (FBS) (Cambrex BioScience, Walkersville, MD), 10⁻⁸M dexamethasone, 10mM β -glycerol 2-phosphate, 50mg/L ascorbic acid, 100mg/L ampicillin, 250mg/L amphotericin, and 50mg/L gentamicin). Complete osteogenic medium without dexamethasone (COM \emptyset dex) was made in the same way but without dexamethasone. Live/Dead viability/cytotoxicity kit was purchased from Molecular Probes (Eugene, OR). The calcium assay was purchased from Genzyme Diagnostics (Cambridge, MA).

1.2.2. Macromer synthesis

Two macromer formulations of statistical copolymers, containing 10 and 13 mol% MAEP, were synthesized as has been previously described.[7] Briefly, statistical copolymers were synthesized from NiPAAm (75.5 or 72.5 mol%), AAm (14.5 mol%), and MAEP (10 or 13 mol%) via AIBN-initiated free radical polymerization in DMSO at 65°C under a nitrogen atmosphere for 20 hours. The product was concentrated by rotoevaporation at 55°C, redissolved in an acetone/DMSO mixture at 9mL/g monomers, added to cold diethyl ether to precipitate the copolymer, vacuum filtered, and dried under vacuum at ambient temperature. The phosphate groups of the macromers were then esterified with GMA at 55°C for 40 hours in the presence of 5000ppm of the radical scavenger butylated hydroxytoluene. The solution was allowed to cool to ambient temperature, diluted with ethanol, precipitated in diethyl ether, and vacuum filtered. The MA-TGM filtrate (a fine white powder) was dried under vacuum at ambient temperature. This process was used to make macromers with a high (13 mol% MAEP formulation) and low (10 mol% MAEP formulation) number of chemically cross-linkable groups to stabilize the hydrogel after thermogelation.

1.2.3. Rat Mesenchymal Stem Cell (MSC) Isolation and Preculture

All procedures followed protocols approved by the Rice University Institutional Animal Care and Use Committee. MSCs were harvested from the marrow of the femora and tibiae of four 6-to-8-week-old male Fischer 344 rats (Harlan Laboratories, Houston, TX) as previously described.[10] The harvested cells were then cultured in COMØdex, with media changes after 24 hours and every 2-3 days afterwards. Following the 6 day preculture period, MSCs were trypsinized, suspended in PBS (pH=7.4) at a concentration of 50 million cells/mL and stored on ice until used.

1.2.4. Hydrogel Formation and Culture

MA-TGM solutions were prepared in PBS (pH 7.4) to give a final concentration of 15% (w/v) after the initiator system and cell solution volumes were added. The groups used for both *in vitro* and *in vivo* experiments are shown in Table 1. For experiments involving COM, the dried MA-TGMs were sterilized with UV radiation for 1 hour prior to dissolution in sterile-filtered PBS (pH=7.4) and placed in medium following fabrication. All solutions were stored on ice prior to mixing. For hydrogels containing MSCs, a stock solution of cells at 50 million cells/mL was added to achieve a final concentration of 15 million cells/mL. Stock solutions of the initiator system in PBS (pH 7.4) were added to the chilled MA-TGM solution to result in final APS and TEMED concentrations of 20mM. The mixture was lightly agitated, and 100µL were pipetted into polytetrafluoroethylene molds (8mm diameter, 2mm height). The molds were incubated at 37°C for 30 minutes to allow the MA-TGMs to thermally and chemically cross-link. This was shortened from 2 hours in previous work[7] to limit the time cells were without nutrients and improve cell viability. After fabrication, the hydrogels were placed in either COM (*in vitro* samples) or COMØdex (*in vivo* samples) and stored at 37°C. For *in vitro* samples, medium was changed at 1 hour after formation and then every 2-3 days afterwards. At the desired time points (days 0, 7, 14, 21, and 28), hydrogels were removed from COM and rinsed with sterile PBS (pH=7.4) three times before analysis. For *in vivo* samples, medium was changed at 1 hour and then stored at 37° C until implantation (6-18 hours after formation). Prior to implantation, hydrogels were rinsed with sterile PBS (pH=7.4).

1.2.1. Live/Dead Staining

At the desired time points, 2-3 independent samples from each group were sliced into ~100µm slices with a hand-held razor blade and incubated for 30 minutes at ambient temperature in PBS containing calcein AM (2µM) and ethidium homodimer-1 (4µM) in accordance with the Live/Dead viability/cytotoxicity kit instructions. The slices were then analyzed using a confocal microscope (LSM 510 META, Carl Zeiss, Germany) using a 10× objective. Argon and helium–neon lasers were used for excitation at 488 and 543 nm, respectively, and emission filters at 505–526 and 612– 644 nm were employed. Representative images of the slices are shown.

1.2.2. Biochemical Assays

The hydrogels to be used for biochemical assays were then placed in 500µL of ultrapure water and stored at -20°C. Before analysis, the samples underwent three freeze-thaw cycles

by alternately immersing in water at ambient temperature and liquid nitrogen, followed by manual homogenation, an additional freeze-thaw cycle, and finally probe ultrasonication for 10 seconds. Aliquots were then taken and used for the assays. The DNA assay was performed according to the manufacturer's instructions. The ALP activity was evaluated with phosphatase substrate capsules in an alkaline buffer solution. The absorbance values were compared to standard solutions of p-nitrophenol. Aliquots for the calcium assay were mixed in equal parts with 1N acetic acid (final concentration 0.5N acetic acid) and incubated on a shaker table overnight at ambient temperature to dissolve the deposited calcium salts. The assay was performed according to the manufacturer's instructions. Each group consisted of n=3-4 independent samples, which were each run in triplicate, and the average of the triplicates was used as the value for that sample. The data are expressed as means and standard deviations of the independent samples from a given group (n=3-4). DNA values were normalized to time-matched acellular hydrogel controls. ALP activity values were normalized to time-matched acellular hydrogel controls and then divided by the normalized DNA from that sample. Values that were outliers based on Grubb's test for outliers were not included in the data sets. Values were analyzed by ANOVA with post-hoc analysis by Tukey's honest significant difference test. Tests were conducted with a 95% confidence interval ($\alpha=0.05$).

1.2.3. *In Vitro* Histological analysis

At the desired timepoints, 2-3 independent samples from each group were fixed in formalin at 37°C for 24 hours. The samples were then dehydrated with 70% ethanol for 24 hours at 37°C and then stored in Histo-Prep for 48 hours at 37°C to allow the freezing medium to permeate the hydrogel. The hydrogels were then frozen at -20°C and longitudinal 10 μ m sections were cut with a cryotome (Leica CM3050S). For von Kossa reagent staining sections were rinsed with ultrapure water, covered with 2% silver nitrate solution, incubated under ultraviolet light for 20 minutes, and then rinsed sequentially with ultrapure water, 5% sodium thiosulfate, ultrapure water, 95% ethanol, and 100% ethanol. Slides were then visualized with a light microscope. Representative images of the slices are shown.

1.2.4. Animal Surgery, Euthanasia, and Implant Harvest

All procedures followed protocols approved by the Rice University Institutional Animal Care and Use Committee. 12-week-old Fischer 344 rats (Harlan Laboratories, Houston, TX) were used for the cranial defect surgeries. Four groups listed in Table 1 were selected for evaluation with 8 implants per group at each of two time points (4 and 12 weeks). Critical-size 8-mm-diameter defects in the rat calvarium were created under general inhalation anesthesia, filled with a preformed hydrogel, then closed, and animals were cared for post-operatively, and euthanized at the desired time points as previously described.[11] Samples for x-ray micro-computed tomography (μ CT) and histology were harvested and fixed in formalin as has been previously described.[11]

1.2.5. μ CT Imaging and Analysis

Both bone volume and extent of bony bridging of the defect were analyzed by SkyScan1172 μ CT (SkyScan, Aartsellar, Belgium) as previously described.[12] The lower binarization threshold index value used was 20, which corresponded to a value that binarized tomograms

most accurately represented their greyscale counterparts in terms of bone morphology. Axial maximum intensity projections were generated and three blinded observers evaluated bony bridging according to the scoring system in Table 2, as has been done previously.[13, 14] Values were analyzed using the Kruskal-Wallis test with post-hoc analysis by the Dwass-Steel-Critchlow-Fligner test. The *a priori* level of significance for the tests was $\alpha=0.05$. All tests were conducted with a 95% confidence interval ($\alpha=0.05$). All quantitative data are expressed as means and standard deviation of all samples from a given group (n=7-8). They were analyzed by ANOVA with post-hoc analysis by Tukey's honest significant difference test.

1.2.1. Histological analysis

Following μ CT analysis, samples were dehydrated in 70% ethanol, embedded in methylmethacrylate, sectioned, and stained using Hematoxylin and eosin (H&E) stain, von Kossa stain, and Goldner's trichrome stain. Light microscopy images of longitudinal center-cut sections were scored by 3 blinded scorers for bony bridging, polymer degradation, and tissue response at the scaffold interface using Table 3, as has been done previously.[13, 14] Tissue response was analyzed at the bone-scaffold interface of each side of the longitudinal, center-cut section (Schematic in Table 3). Scores for the extent of bony bridging and the scaffold degradation are expressed as means and standard deviations of all samples from a given group, and were analyzed using the Kruskal-Wallis test with post-hoc analysis by the Dwass-Steel-Critchlow-Fligner test. The *a priori* level of significance for the tests was $\alpha=0.05$. Scores for the tissue response at the bone scaffold interface (n=14-16) were analyzed using a repeated measures ANOVA ($\alpha=0.05$) to account for the non-independence of scores from each edge of the same sample. Representative images of a sample from each group (n=7-8 independent samples) are shown in Figure 9.

1.3. Results

1.3.1. Hydrogel Formation and MSCs Encapsulation

Stable hydrogels both with and without encapsulated MSCs were successfully fabricated. Hydrogels were incubated for 30 minutes in polytetrafluoroethylene molds at 37°C prior to incubation in PBS remained stable after formation, with swelling ratios around 5 (slightly larger than those reported when a 2 hour incubation period was used).[7]

Figure 1 shows representative images of cross sections of cell-laden hydrogels taken on the confocal fluorescence microscope. The images show that MSCs were dispersed throughout the entire thickness of the hydrogel. The encapsulation process resulted in very little cell death, as the vast majority of the cells stained green (live) and only a few stained red (dead) at the day 0 time point 2 hours after encapsulation. Furthermore, evaluation at later time points showed that viable cells could be visualized within the center of the hydrogel for all time points.

1.3.1. Biochemical Assay Analyses

Figure 2 shows the DNA content of homogenized hydrogels over 28 days in COM. While DNA content decreased with time, DNA could still be detected at the day 28 time point. At

each time point, no differences were observed in cell viability between the two hydrogel formulations.

Production of ALP is a marker for osteogenic differentiation of MSCs. Figure 3 illustrates the ALP activity per ng DNA of the homogenized hydrogels over time. Both hydrogel formulations show significant increases in ALP activity with time, indicating some of the encapsulated MSCs were undergoing osteogenesis. 13 mol% MAEP hydrogels demonstrated levels significantly higher than hydrogels of the same formulation at day 0 earlier (day 21) than the 10 mol% MAEP hydrogels (day 28).

As shown in Figure 4, MSC-laden hydrogels exhibited significant mineralization over time, while acellular hydrogels did not increase calcium content significantly, indicating cellular activity is necessary for facilitating mineralization of these hydrogels. Main effects analysis showed that mol% MAEP had no statistically significant effect on calcium content.

Figure 5 shows histological sections of both cell-laden and acellular hydrogels. The mineralization of the cell-laden hydrogels increases with time, which supports the quantitative data presented in Figure 4.

1.3.2. Animal Care

Surgery was performed on 64 rats, of which one animal (13 mol% MAEP cell-laden hydrogel) died at 11 weeks and was excluded from statistical analysis. The cause of death was unknown, but histological evaluation of the defect site revealed no apparent local pathology, and high bone regeneration scores (3 on histological bony bridging, 3 on μ CT bony bridging 8.6% bone volume by μ CT). Three animals developed scabs over the defect area between 3 and 5 weeks post-op (two 10 mol% MAEP cell-laden hydrogel and one 10 mol% MAEP acellular hydrogel), but did not appear to be in any pain so they were euthanized as scheduled and were included in all analyses. One rat was euthanized as scheduled at 4 weeks before the wound healed and the others completely healed prior to scheduled euthanasia at 12 weeks. Two of these animals (both 10 mol% MAEP cell-laden hydrogels) had inflammation around the scaffold on histological slides marked by an abundance of inflammatory cells and poorly organized tissue, but were still included in all statistical analyses. One animal (10 mol% MAEP acellular hydrogel at 12 weeks) was excluded after harvest because the hydrogel implant had dislocated from the defect site post operatively. One set of histological slides (13 mol% MAEP acellular hydrogel at 4 weeks) contained sectioning artifacts at 1 of bone scaffold interfaces, so only 1 side was scored (which received a score of 4).

1.3.3. μ CT Analysis

Figure 6 shows the % bone volume of the defects for each group. At 4 weeks, the cell-laden 13 mol% MAEP hydrogels had significantly more bone volume than the acellular 10 mol% MAEP hydrogels. At 12 weeks, no statistically significant differences were seen between groups. Main effects analysis revealed neither mol% MAEP nor the presence of cells had a statistically significant effect on bone volume, but bone volume did increase with time.

Figure 7 shows the results of the μ CT analysis of bony bridging scores across the defect according to the criteria in Table 3. While no statistically significant differences were seen between groups, main effects analysis revealed that the higher mol% MAEP resulted in significantly improved bony bridging. No other factors were shown to have a significant effect.

1.3.1. Histological Analysis

Figure 8 presents the results of histological analysis of bony bridging across the defect according to the criteria in Table 3. Main effects analysis revealed bony bridging increased significantly with the higher level of MAEP and with the presence of encapsulated MSCs. Appropriately, main effects analysis showed the group with cell-laden 13 mol% MAEP hydrogels had significantly higher bony bridging scores than all other groups. Figure 9 shows representative images of histological sections of samples from each group, which demonstrate bone growth into the defect site in both cell-laden and acellular hydrogels. Figure 10 shows mineralization around cells that were encapsulated within the hydrogels.

Figure 11 demonstrates the hydrogels degrading with time within the defect, as scored by Table 3. There were no significant differences in extent of degradation between groups at the same time point. Main effects analysis indicated the level of MAEP and the presence of encapsulated cells had no statistical effect on degradation score, though the score increased significantly with time.

Figure 12.A illustrates a hydrogel that has undergone excessive fragmentation and degradation allowing host tissue to infiltrate the hydrogel, with bone making direct contact and surrounding some fragments. At higher magnifications blood vessels can be visualized infiltrating hydrogels in addition to bone tissue, as shown in Figure 12.B.

Figure 13 shows the scores of the histological response at the scaffold interfaces (2 per sample) according to the criteria in Table 3. When evaluating across all time points, 20 of the 31 (65%) 13 mol% MAEP samples evaluated demonstrated direct bone-to-implant contact, while 15 of the 31 (48%) 10 mol% MAEP samples evaluated demonstrated direct bone-to-implant contact. 19 of the 31 (61%) cell-laden samples evaluated demonstrated direct bone-to-implant contact, while 16 of the 31 (52%) acellular samples evaluated demonstrated direct bone-to-implant contact. Additionally, minimal fibrous capsule formation was observed, with only 3 of the 123 (2.4%) interfaces scored receiving a score of 2. Histological scores did not differ significantly between formulations when evaluated across all time points. However, cell-laden hydrogels demonstrated significantly more direct bone-implant contact than acellular hydrogels ($p=0.0004$), and cell-laden 13 mol% MAEP hydrogels had significantly more direct bone-implant contact than the other 3 formulations ($p=0.0002$) when evaluated across all time points.

1.4. Discussion

The dual-gelling macromer system was synthesized and evaluated for osteogenic potential both *in vitro* and *in vivo*. The *in vitro* studies set out to evaluate the ability of two dual-gelling macromers to encapsulate rat MSCs and characterize the cell viability, osteogenic

differentiation, and mineralization under osteogenic conditions. Both the 10 mol% and 13 mol% MAEP macromers underwent dual thermal and chemical gelation to encapsulate MSCs within stable hydrogels. Confocal microscopy revealed the cells were uniformly distributed within both hydrogel formulations and demonstrated that cells could remain viable within them for up to 28 days. Viability of cells within the hydrogels was supported quantitatively by the DNA detection in both hydrogel formulations at the day 28 time point. The DNA content did decrease with time, which is seen commonly in hydrogels made from synthetic polymers such as poly(ethylene glycol)[15] and oligo(poly(ethylene glycol) fumarate).[16, 17] The decrease in detected DNA could be caused by the lack of natural binding sites for cells encapsulated within the hydrogel, and incorporation of natural binding sites could improve the hydrogel's ability to sustain viable cells.[18] Over the 28 days, the osteogenic marker ALP increased with time, indicating the cells within the hydrogel were undergoing osteogenic differentiation. Similar trends have been seen in oligo(poly(ethylene glycol) fumarate)/calcium phosphate nanocomposites.[19] While the cell viability and osteogenic differentiation showed similar results to many other synthetic hydrogels, a major advantage of the hydrogels discussed in this study is their ability to rapidly (in a matter of seconds rather than minutes to hours) form *in situ*, making them more viable for cell-delivery applications into irregularly shaped defects. This macromer system represents a promising step forward for the use of thermogelling polymers for cell-delivery applications, which has been limited previously by syneresis.

The calcium assay results also indicated cell-laden hydrogels underwent significant mineralization with time. The values from the calcium assay for cell-laden hydrogels were similar to cell-laden oligo(poly(ethylene glycol) fumarate) hydrogels[16] and cell-laden phosphorylated poly(ethylene glycol) hydrogels[20] under osteogenic conditions. However, the results from the calcium assay revealed that acellular hydrogels did not significantly mineralize within COM. This result differs from previous hydrogel mineralization studies[7] with the same formulations that allowed 2 hours incubation time within polytetrafluoroethylene molds for hydrogels to chemically cross-link before placing them in media. Incubating within the polytetrafluoroethylene molds for 30 minutes could result in relatively shorter kinetic chain lengths and increased reactions (such as chain transfer) with contents of the media. Either of these proposed mechanisms could lead to a decrease in the number of hydrophobic chains or hydrophobic chain lengths within the hydrogels, which may reduce protein binding and subsequent mineralization. A decrease in hydrophobicity when using a shorter incubation period is further supported by the slightly larger swelling ratios found with 30 minute incubation periods compared to 2 hour incubation periods,[7] as a relative decrease in hydrophobicity of macromer chains has been shown to result in greater water retention within hydrogels.[21] In spite of the more hydrophilic environment, cell-laden hydrogels underwent significant mineralization as seen by the calcium assay of hydrogel sections. In addition to secreting and mineralizing extracellular matrix, cells undergoing osteogenic differentiation also produce ALP, which has been shown previously to accelerate degradation of these hydrogels.[7] Moving forward, the system could be improved by enhancing cell viability and subsequent osteogenic differentiation by incorporation of cell-binding domains and osteogenic growth factors, which would accelerate hydrogel degradation via increased total ALP production.

The *in vivo* study set out to evaluate the ability of both cell-laden and acellular hydrogels formed from dual-gelling macromers to facilitate bone growth within a critical-size rat cranial defect as well as assess the ability of hydrogels to undergo *in vivo* degradation. Bone volume within the defect after 12 weeks measured by μ CT averaged approximately 9% across all groups, which was similar to that of porous poly(lactic acid) scaffolds seeded with marrow mononuclear cells encapsulated within fibrin glue[13] and poly(propylene fumarate)/alumoxane nanocomposites.[14] The bony bridging scores were also similar to those in previous studies. The present study demonstrated that the higher level of MAEP resulted in significantly more bony bridging of the defect, both by histological and μ CT analyses. Improved bony bridging in hydrogels with higher levels of MAEP could indicate that increased phosphate content can help facilitate guided bone growth across the hydrogel surface. Additionally, this study demonstrated the ability of this macromer system to deliver and support stem cells within a cranial defect, and the presence of cells significantly improved bony bridging as scored by histological analysis. Presence of cells seemed to have a larger impact at early time points, before the native tissues infiltrate the hydrogels.

One area where this study performed better than many other scaffolds previously used was direct bone contact with the scaffold, which was rarely observed in other studies.[12, 13, 22, 23] Hydrogels implanted in rat cranial defects in previous studies were often surrounded by fibrous tissue, and required use of growth factors, encapsulated cells, or mineral composites to facilitate infiltration of bone tissue.[23–27] Contrastingly, the majority of hydrogels used in the study described in this manuscript, including the subset of acellular hydrogels, demonstrated direct bone-to-implant contact with bone infiltration into the hydrogel, rather than the fibrous tissue response commonly associated with biomaterials implanted into the body.[28] Bone tissue infiltrating into the hydrogels indicates these hydrogels have the potential to integrate with host tissue and accelerate bone formation, and may be a consequence of improved cellular interactions secondary to the presence of phosphate groups in both of the hydrogel formulations used. Cell encapsulation resulted in significantly more direct bone contact with scaffolds, and the cell-laden hydrogels with a higher level of MAEP had significantly more direct bone contact than other groups. The improved tissue integration may be a consequence of encapsulated cells accelerating degradation, laying down extracellular matrix at the interface, and, in combination with phosphate groups, facilitating binding and infiltration of osteogenic cells. Another major strength of the hydrogels in this study was their ability to undergo *in vivo* degradation. All groups of hydrogels demonstrated degradation within the defect. Degradability is vital for tissue engineering applications, as it allows for tissue ingrowth into the hydrogel and eventual replacement of the hydrogel with host tissues. Histological sections revealed that bone tissue as well as blood vessels infiltrated the hydrogels (Figure 12), demonstrating the osteogenic potential of these hydrogels.

Notably, the *in vivo* study demonstrated that cells in close proximity to bone tissue mineralized much more than those further away from bone tissue. The lack of mineralization near the center of the hydrogels indicates that the phosphate groups present on the macromers in combination with endogenous growth factors were not adequate stimuli to facilitate osteogenic differentiation in cells located within the center of the hydrogel. It is

likely the cells further from newly formed bone tissue did not receive the signals necessary to direct them down an osteoblastic lineage. Consequently, inclusion of signals that would direct MSCs down an osteoblastic lineage within the hydrogel may further improve bone regeneration.

1.5. Conclusions

The biological interactions of a novel, dual-gelling macromer with the potential for delivering cells through *in situ* formation of hydrogels was investigated. These dual-gelling macromers were shown to undergo rapid dual gelation to form stable hydrogels that encapsulated MSCs with little cell death and supported cells for up to 28 days *in vitro*, during which markers of osteogenic differentiation were detected. Furthermore, cell-laden hydrogels were shown to undergo significant mineralization, making these macromers a promising system for craniofacial bone tissue engineering, and a candidate for *in vivo* evaluation. The *in vivo* study demonstrated the ability of dual-gelling, phosphate containing hydrogels to deliver MSCs and facilitate bone growth within a critical-size rat cranial defect. While these hydrogels facilitated bone growth similarly to other previously reported scaffolds, the hydrogels discussed in this study have the potential to form *in situ*. Therefore, they can be used to fill irregularly shaped defects common in the craniofacial area. Furthermore, these hydrogels were shown to readily degrade within the defect, allowing for infiltration of host tissue and bone tissue formation within fragmented hydrogels. Finally, this hydrogel system demonstrated excellent integration with host bone tissue, as demonstrated by direct bone-to-implant contact, and consequently, this hydrogel system warrants further investigation for use in craniofacial bone tissue engineering.

Acknowledgments

We acknowledge support by the National Institutes of Health (R01 DE17441 and R01 AR48756), the Keck Center Nanobiology Training Program of the Gulf Coast Consortia (NIH Grant No. T32 EB009379), and the Baylor College of Medicine Medical Scientist Training Program (NIH T32 GM007330).

References

1. Ward BB, Brown SE, Krebsbach PH. Bioengineering strategies for regeneration of craniofacial bone: a review of emerging technologies. *Oral Dis.* 2010; 16:709–16.10.1111/j.1601-0825.2010.01682.x [PubMed: 20534013]
2. Kretlow JD, Young S, Klouda L, Wong M, Mikos AG. Injectable biomaterials for regenerating complex craniofacial tissues. *Adv Mater.* 2009; 21:3368–93.10.1002/adma.200802009 [PubMed: 19750143]
3. Drury JL, Mooney DJ. Hydrogels for tissue engineering: scaffold design variables and applications. *Biomaterials.* 2003; 24:4337–51.10.1016/S0142-9612(03)00340-5 [PubMed: 12922147]
4. Hunt NC, Grover LM. Cell encapsulation using biopolymer gels for regenerative medicine. *Biotechnol Lett.* 2010; 32:733–42.10.1007/s10529-010-0221-0 [PubMed: 20155383]
5. Wei CC, Lin AB, Hung SC. Mesenchymal stem cells in regenerative medicine for musculoskeletal diseases: bench, bedside, and industry. *Cell Transplant.* 2014; 23:505–12.10.3727/096368914X678328 [PubMed: 24816447]
6. Gan T, Guan Y, Zhang Y. Thermogelable PNIPAM microgel dispersion as 3D cell scaffold: effect of syneresis. *J Mater Chem.* 2010; 20:5937.10.1039/c0jm00338g
7. Watson BM, Kasper FK, Engel PS, Mikos AG. Synthesis and characterization of injectable, biodegradable, phosphate-containing, chemically cross-linkable, thermoresponsive macromers for

- bone tissue engineering. *Biomacromolecules*. 2014; 15:1788–96.10.1021/bm500175e [PubMed: 24758298]
8. Lutolf MP, Lauer-Fields JL, Schmoekel HG, Metters AT, Weber FE, Fields GB, et al. Synthetic matrix metalloproteinase-sensitive hydrogels for the conduction of tissue regeneration: engineering cell-invasion characteristics. *Proc Natl Acad Sci U S A*. 2003; 100:5413–8.10.1073/pnas.0737381100 [PubMed: 12686696]
 9. Watson BM, Kasper FK, Mikos AG. Phosphorous-containing polymers for regenerative medicine. *Biomed Mater*. 2014; 9:025014.10.1088/1748-6041/9/2/025014 [PubMed: 24565855]
 10. Thibault RA, Scott Baggett L, Mikos AG, Kasper FK. Osteogenic differentiation of mesenchymal stem cells on pregenerated extracellular matrix scaffolds in the absence of osteogenic cell culture supplements. *Tissue Eng Part A*. 2010; 16:431–40.10.1089/ten.TEA.2009.0583 [PubMed: 19863274]
 11. Patel ZS, Young S, Tabata Y, Jansen JA, Wong MEK, Mikos AG. Dual delivery of an angiogenic and an osteogenic growth factor for bone regeneration in a critical size defect model. *Bone*. 2008; 43:931–40.10.1016/j.bone.2008.06.019 [PubMed: 18675385]
 12. Young S, Patel ZS, Kretlow JD, Murphy MB, Mountziaris PM, Baggett LS, et al. Dose effect of dual delivery of vascular endothelial growth factor and bone morphogenetic protein-2 on bone regeneration in a rat critical-size defect model. *Tissue Eng Part A*. 2009; 15:2347–62.10.1089/ten.tea.2008.0510 [PubMed: 19249918]
 13. Kretlow JD, Spicer PP, Jansen JA, Vacanti CA, Kasper FK, Mikos AG. Uncultured marrow mononuclear cells delivered within fibrin glue hydrogels to porous scaffolds enhance bone regeneration within critical-sized rat cranial defects. *Tissue Eng Part A*. 2010; 16:3555–68.10.1089/ten.TEA.2010.0471 [PubMed: 20715884]
 14. Mistry AS, Pham QP, Schouten C, Yeh T, Christenson EM, Mikos AG, et al. In vivo bone biocompatibility and degradation of porous fumarate-based polymer/alumoxane nanocomposites for bone tissue engineering. *J Biomed Mater Res A*. 2010; 92:451–62.10.1002/jbm.a.32371 [PubMed: 19191316]
 15. Chatterjee K, Lin-Gibson S, Wallace WE, Parekh SH, Lee YJ, Cicerone MT, et al. The effect of 3D hydrogel scaffold modulus on osteoblast differentiation and mineralization revealed by combinatorial screening. *Biomaterials*. 2010; 31:5051–62.10.1016/j.biomaterials.2010.03.024 [PubMed: 20378163]
 16. Temenoff JS, Park H, Jabbari E, Sheffield TL, LeBaron RG, Ambrose CG, et al. In vitro osteogenic differentiation of marrow stromal cells encapsulated in biodegradable hydrogels. *J Biomed Mater Res A*. 2004; 70:235–44.10.1002/jbm.a.30064 [PubMed: 15227668]
 17. Park H, Temenoff JS, Tabata Y, Caplan AI, Mikos AG. Injectable biodegradable hydrogel composites for rabbit marrow mesenchymal stem cell and growth factor delivery for cartilage tissue engineering. *Biomaterials*. 2007; 28:3217–27.10.1016/j.biomaterials.2007.03.030 [PubMed: 17445882]
 18. Shin H, Zygourakis K, Farach-Carson MC, Yaszemski MJ, Mikos AG. Attachment, proliferation, and migration of marrow stromal osteoblasts cultured on biomimetic hydrogels modified with an osteopontin-derived peptide. *Biomaterials*. 2004; 25:895–906.10.1016/S0142-9612(03)00602-1 [PubMed: 14609678]
 19. Bongio M, van den Beucken JJJP, Nejadnik MR, Leeuwenburgh SCG, Kinard LA, Kasper FK, et al. Biomimetic modification of synthetic hydrogels by incorporation of adhesive peptides and calcium phosphate nanoparticles: in vitro evaluation of cell behavior. *Eur Cell Mater*. 2011; 22:359–76. [PubMed: 22179935]
 20. Wang DA, Williams CG, Yang F, Cher N, Lee H, Elisseff JH. Bioresponsive phosphoester hydrogels for bone tissue engineering. *Tissue Eng*. 2005; 11:201–13.10.1089/ten.2005.11.201 [PubMed: 15738675]
 21. Hacker MC, Klouda L, Ma BB, Kretlow JD, Mikos AG. Synthesis and characterization of injectable, thermally and chemically gelable, amphiphilic poly(N-isopropylacrylamide)-based macromers. *Biomacromolecules*. 2008; 9:1558–70.10.1021/bm8000414 [PubMed: 18481893]
 22. Chew SA, Kretlow JD, Spicer PP, Edwards AW, Baggett LS, Tabata Y, et al. Delivery of plasmid DNA encoding bone morphogenetic protein-2 with a biodegradable branched polycationic

- polymer in a critical-size rat cranial defect model. *Tissue Eng Part A*. 2011; 17:751–63.10.1089/ten.TEA.2010.0496 [PubMed: 20964581]
23. Vo TN, Ekenseair AK, Spicer PP, Watson BM, Tzouanas SN, Roh TT, et al. In vitro and in vivo evaluation of self-mineralization and biocompatibility of injectable, dual-gelling hydrogels for bone tissue engineering. *J Control Release*. 2014.10.1016/j.jconrel.2014.11.028
 24. Kasper FK, Young S, Tanahashi K, Barry MA, Tabata Y, Jansen JA, et al. Evaluation of bone regeneration by DNA release from composites of oligo(poly(ethylene glycol) fumarate) and cationized gelatin microspheres in a critical-sized calvarial defect. *J Biomed Mater Res A*. 2006; 78:335–42.10.1002/jbm.a.30698 [PubMed: 16639744]
 25. Kim J, Kim IS, Cho TH, Lee KB, Hwang SJ, Tae G, et al. Bone regeneration using hyaluronic acid-based hydrogel with bone morphogenic protein-2 and human mesenchymal stem cells. *Biomaterials*. 2007; 28:1830–7.10.1016/j.biomaterials.2006.11.050 [PubMed: 17208295]
 26. Patterson J, Siew R, Herring SW, Lin ASP, Guldborg R, Stayton PS. Hyaluronic acid hydrogels with controlled degradation properties for oriented bone regeneration. *Biomaterials*. 2010; 31:6772–81.10.1016/j.biomaterials.2010.05.047 [PubMed: 20573393]
 27. Tan R, Feng Q, Jin H, Li J, Yu X, She Z, et al. Structure and Biocompatibility of an Injectable Bone Regeneration Composite. *J Biomater Sci Polym Ed*. 2011; 22:1861–79.10.1163/092050610X528561 [PubMed: 20979688]
 28. Anderson JM, Rodriguez A, Chang DT. Foreign body reaction to biomaterials. *Semin Immunol*. 2008; 20:86–100.10.1016/j.smim.2007.11.004 [PubMed: 18162407]

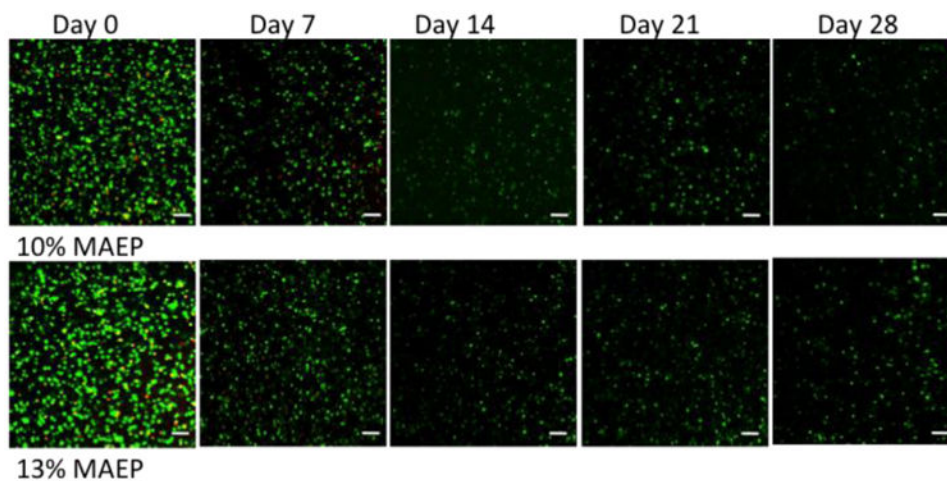


Figure 1. Confocal fluorescence microscopy representative images of sections taken from the center of the hydrogels stained with Live/Dead reagent at various time points. Live cells fluoresce green and dead cells stain red. Autofluorescence of the hydrogels at the wavelengths used for the dead dye component was observed after day 7 and therefore the images for days 14-28 only show the live stain. Rat MSCs were encapsulated in hydrogels composed of 10 and 13 mol% MAEP and incubated in complete osteogenic medium until the desired time point. Scale bar = 100µm.

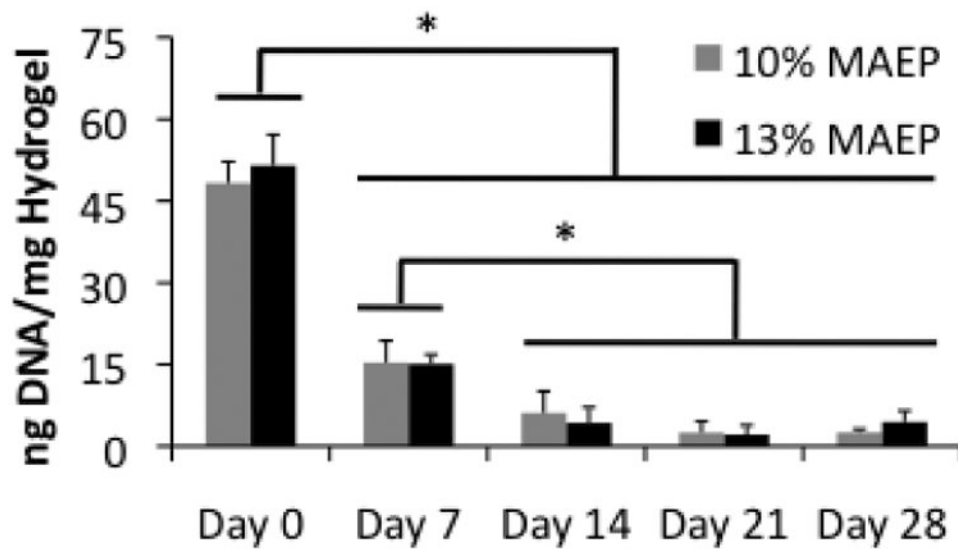


Figure 2. DNA content of homogenized hydrogels composed of 10 and 13 mol% MAEP used to encapsulate rat MSCs and incubated in complete osteogenic medium for 0, 7, 14, 21, and 28 days. * indicates that the groups are significantly different from one another ($p < 0.05$). Error bars show standard deviation ($n=4$).

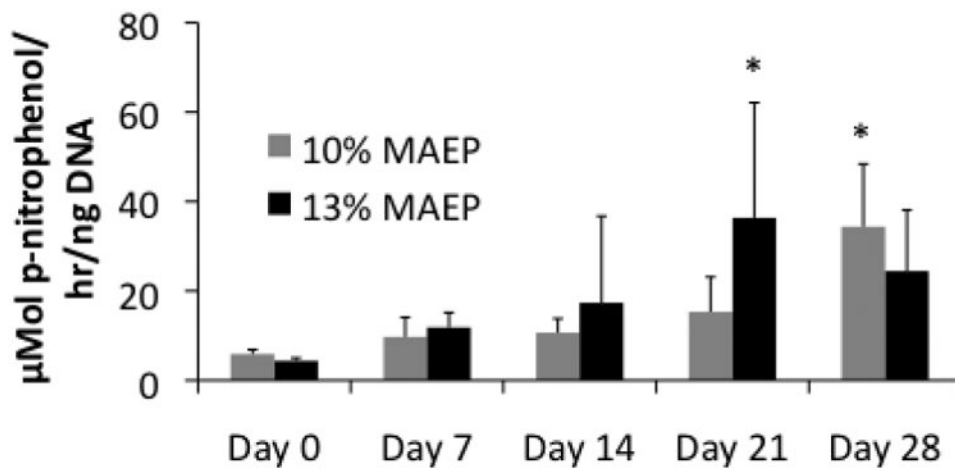


Figure 3. Alkaline phosphatase activity of homogenized hydrogels composed of 10 and 13 mol% MAEP used to encapsulate rat MSCs and incubated in complete osteogenic medium for 0, 7, 14, 21, and 28 days. * indicates that the values are significantly larger than the corresponding Day 0 values within a group ($p < 0.05$). Error bars show standard deviation ($n=3-4$).

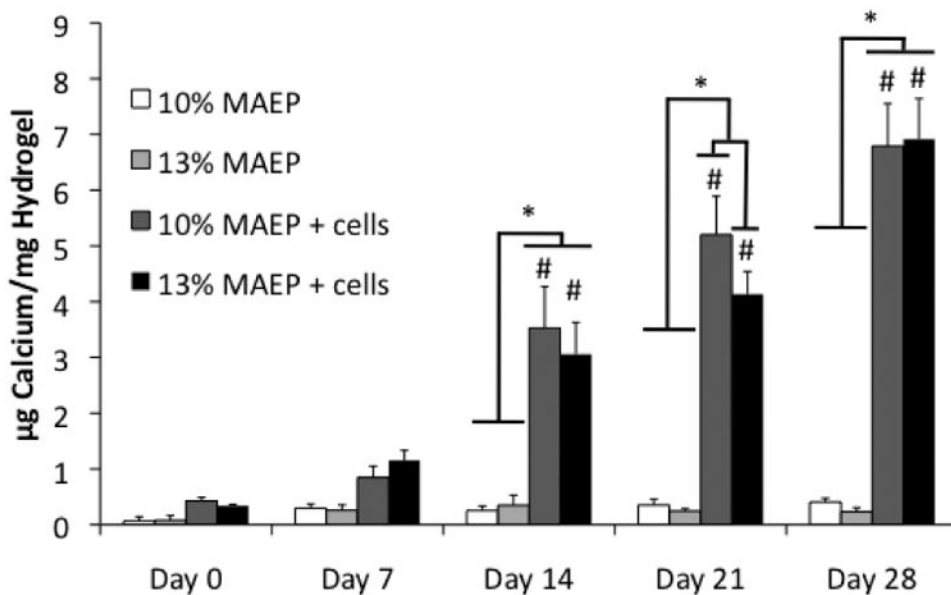


Figure 4. Calcium content of homogenized hydrogels composed of 10 and 13 mol% MAEP with and without rat MSCs. Hydrogels were incubated in complete osteogenic medium until the desired time point. * indicates that the values are significantly different from others at a time point ($p < 0.05$). # indicates that the point is significantly greater than previous time points within a group. Error bars show standard deviation ($n=4$).

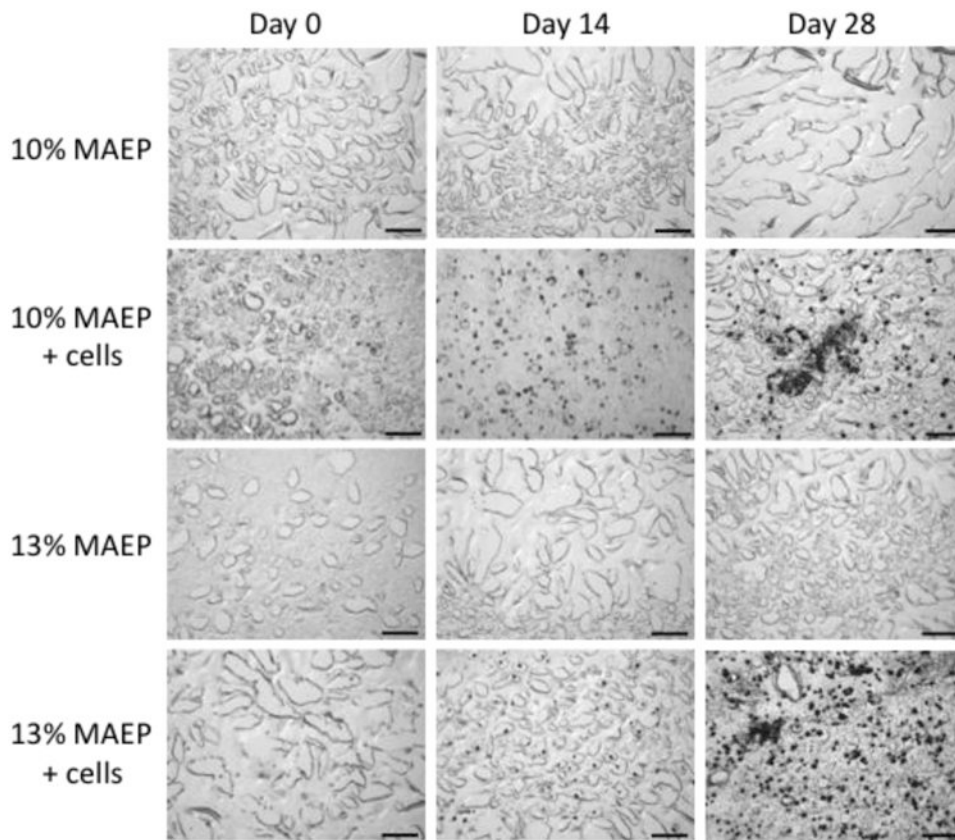


Figure 5. Representative histological sections (von Kossa stain- mineralized tissue stains black) of center-cut sections of hydrogels composed of 10 and 13 mol% MAEP with and without rat MSCs. Hydrogels were incubated in complete osteogenic medium until the desired time point. Scale bar is 100 μ m.

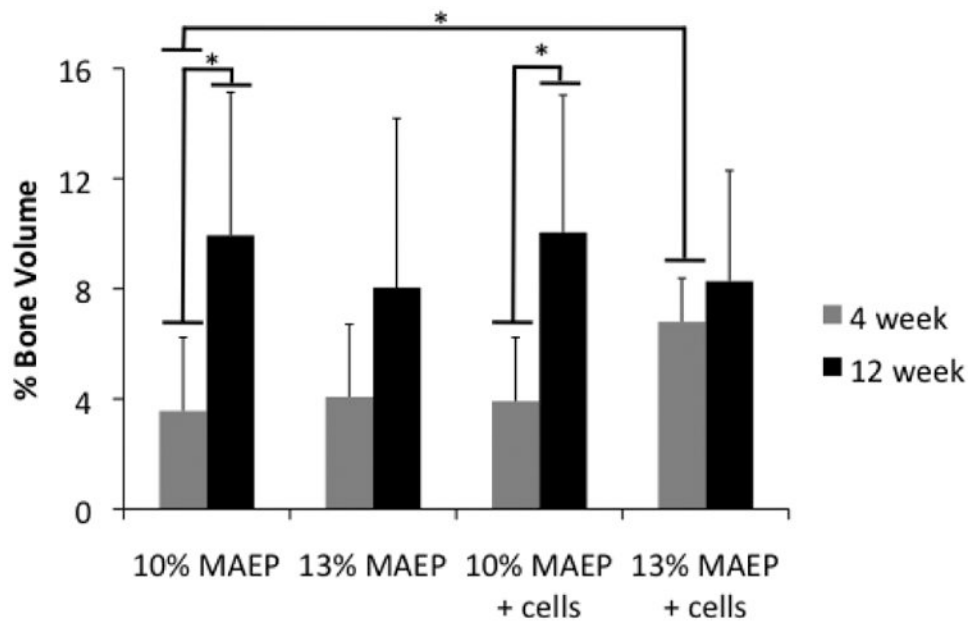


Figure 6. Bone volume within the defect measured by μ CT. * indicates that the groups are significantly different from one another ($p < 0.05$). Error bars show standard deviation ($n=7-8$).

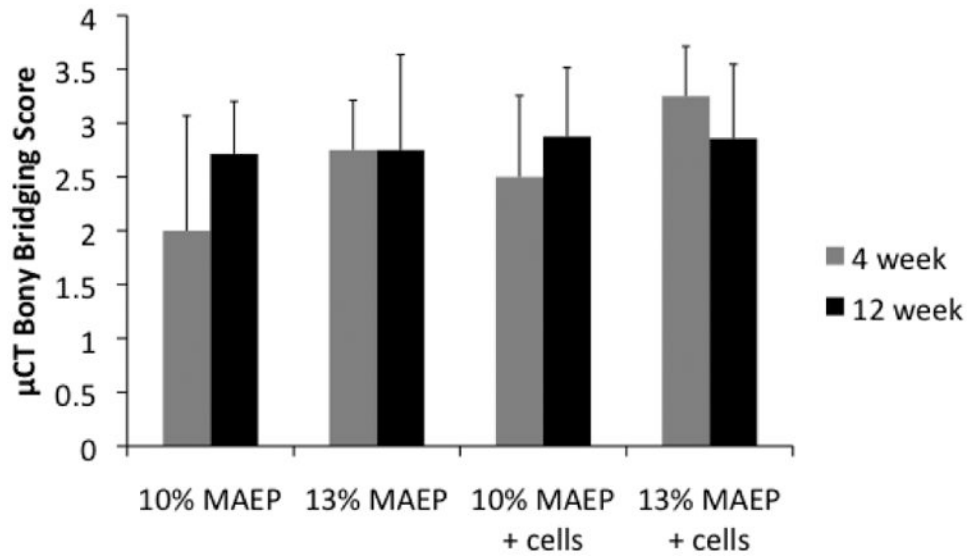


Figure 7. Scores of μ CT analysis of bony bridging and union of the defect. Error bars show standard deviation (n=7-8).

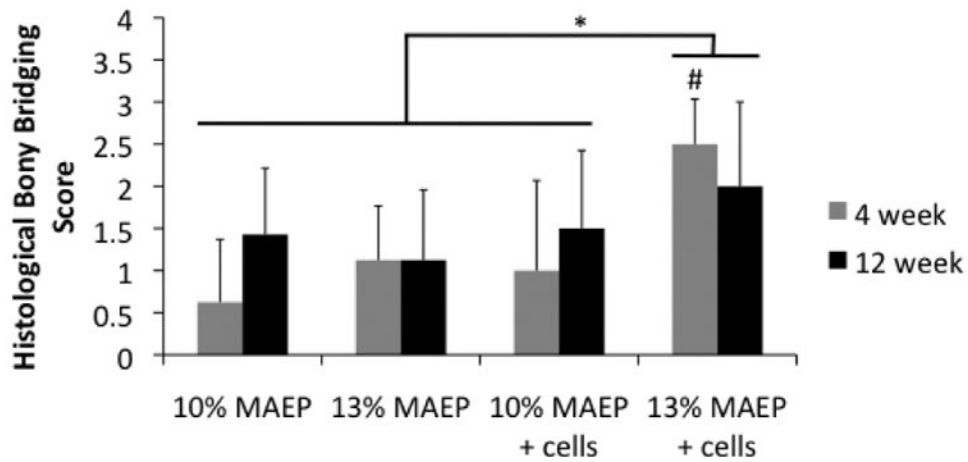


Figure 8. Scores of histological analysis of bony bridging across the defect. # indicates that the point is significantly different than other groups within a time point ($p < 0.05$). * indicates the main effects analysis showed 13 mol% MAEP + cells group has significantly higher bony bridging scores when evaluated across all time points ($p < 0.05$). Error bars show standard deviation ($n = 7-8$).

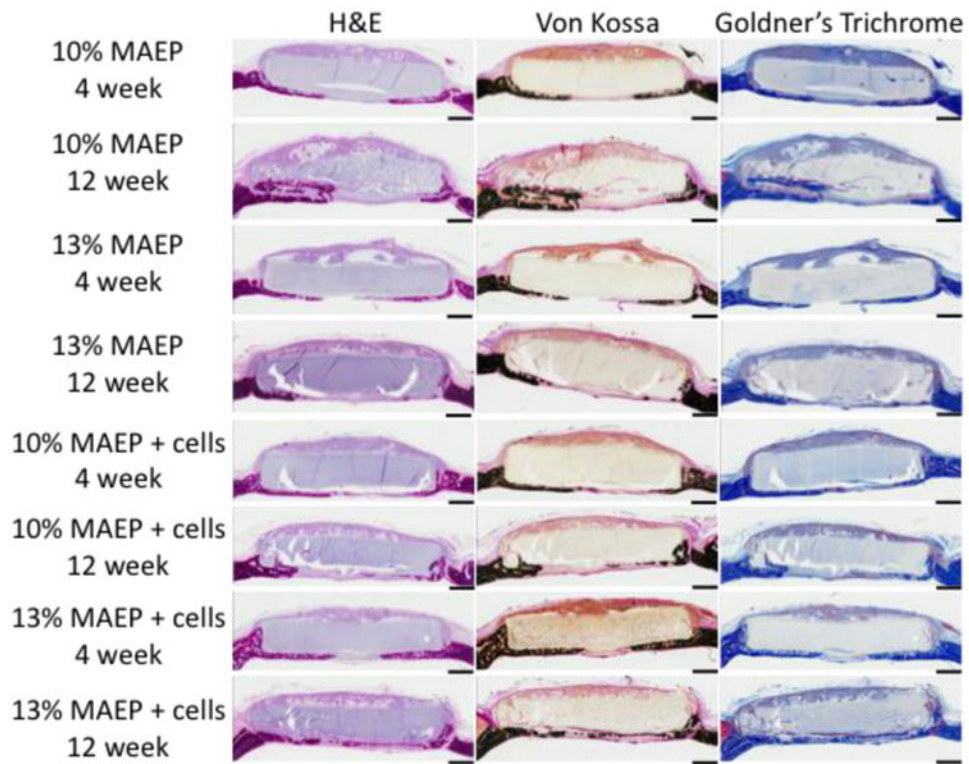


Figure 9. Representative histological sections of H&E stain, von Kossa stain and Goldner's Trichrome stain of hydrogels composed of 10 and 13 mol% MAEP with and without rat MSCs at the 4 and 12 week time points. Scale bar is 1mm.

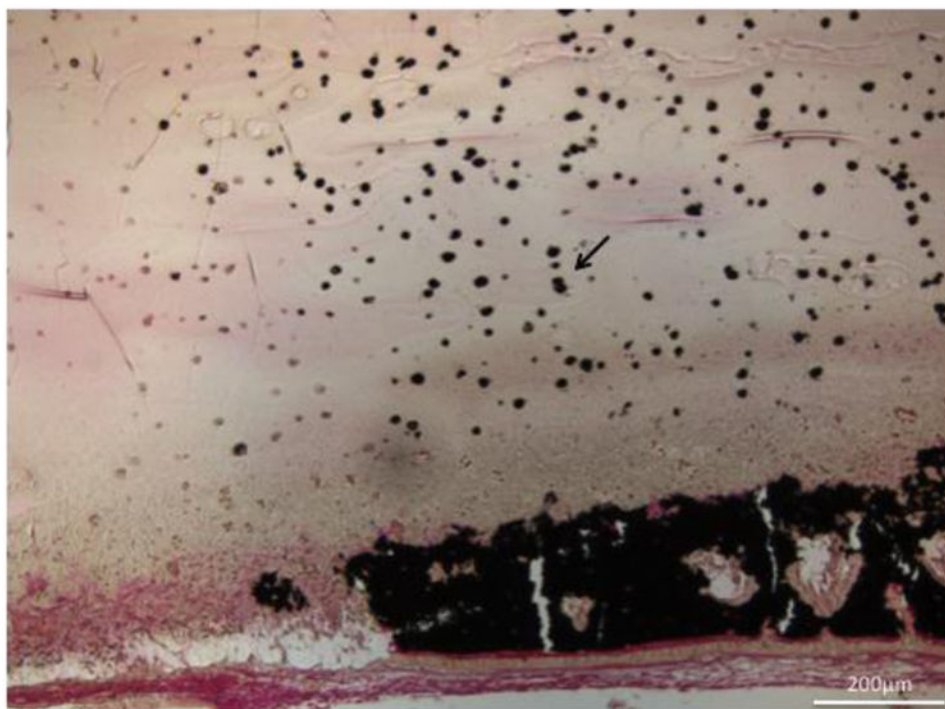


Figure 10. Histological section (von Kossa stain- mineralized tissue stains black) of cell induced mineralization within a 13 mol% MAEP cell-laden hydrogel (arrow) at the 4 week timepoint. Scale bar is 200μm.

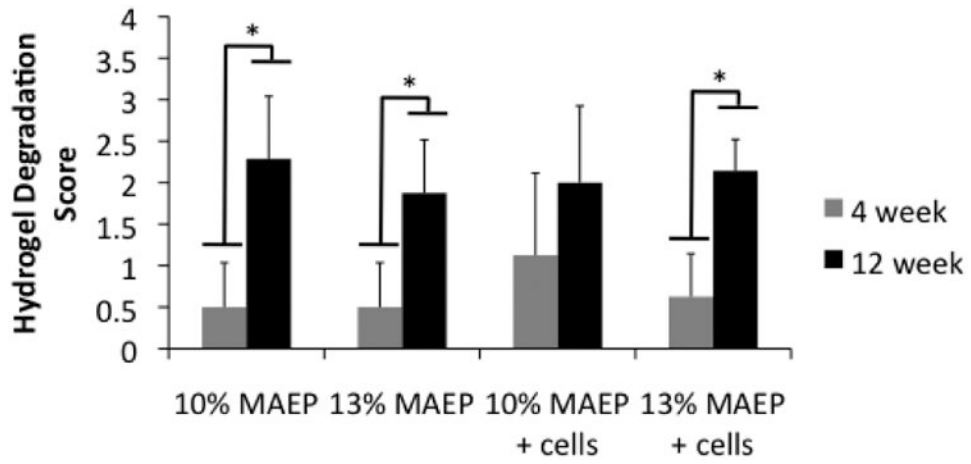


Figure 11. Scores of histological analysis of hydrogel degradation. * indicates that the groups are significantly different from one another ($p < 0.05$). Error bars show standard deviation ($n = 7-8$).

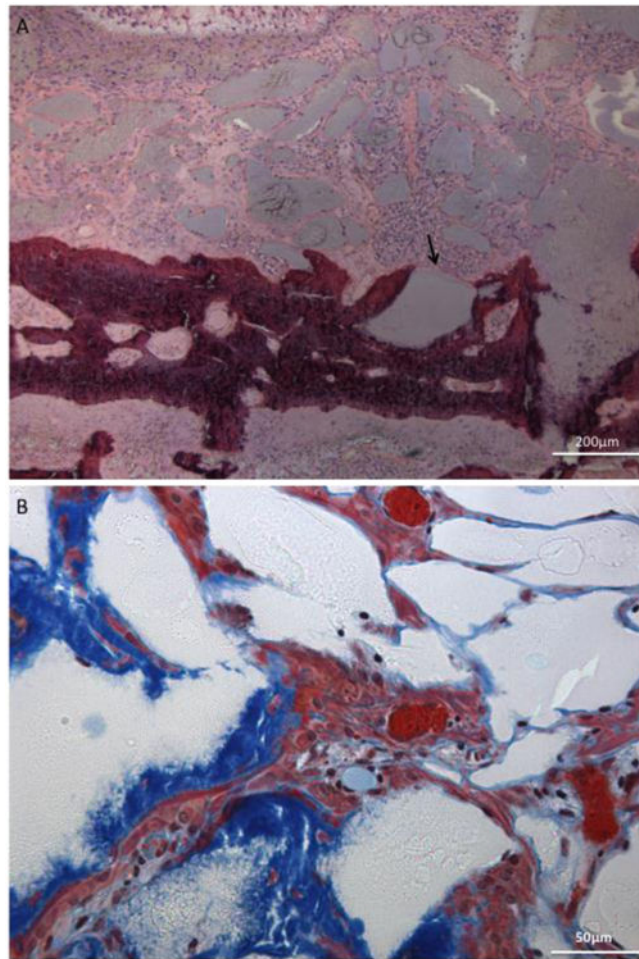


Figure 12.

A) Histological section (H&E stain) of 13 mol% MAEP acellular hydrogel fragmentation (arrow) and degradation adjacent to newly formed bone (dark purple) at the 12 week timepoint and B) histological section (Goldner's Trichrome stain) of 10 mol% MAEP acellular hydrogel demonstrating bone infiltration (blue) and blood vessel formation (orange) within a fragmented hydrogel (white) at the 12 week timepoint. Scale bar is 200µm in A) and 50µm in B).

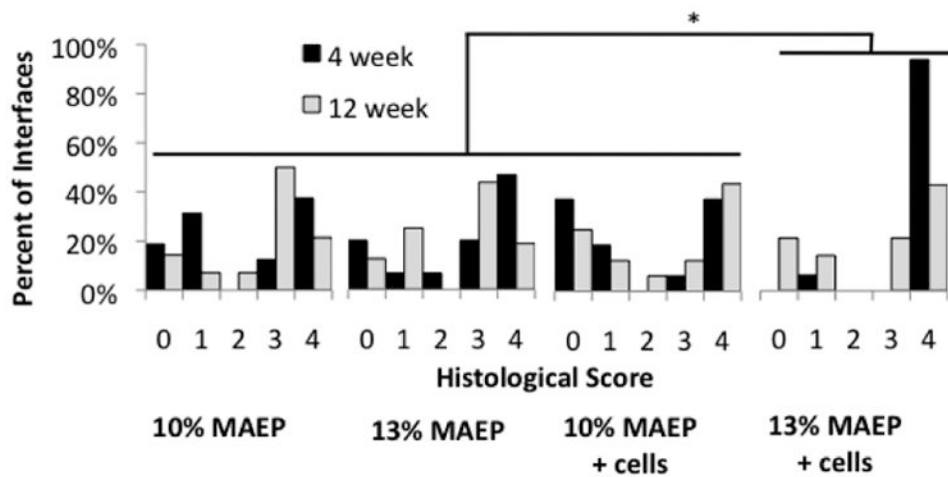


Figure 13. Scores of histological analysis of tissue response at the bone-scaffold interface using longitudinal center-cut histological sections. * indicates the 13 mol% MAEP + cells group has significantly more direct bone-to-implant contact (score=4) than the other 3 groups ($p=0.0002$) when evaluated across all time points.

Table 1

Combinations of the experimental levels of monoacryloxyethyl phosphate (MAEP) mole percentage and mesenchymal stem cell (MSC) density used for hydrogel *in vitro* and *in vivo* characterization.

Group	MAEP	MSCs
A	10 mol%	0 cells/mL
B	13 mol%	0 cells/mL
C	10 mol%	15 million cells/mL
D	13 mol%	15 million cells/mL

Author Manuscript

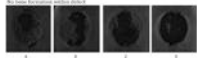
Author Manuscript

Author Manuscript

Author Manuscript

Table 2

Scoring guide for the extent of bony bridging and union of defects evaluated by maximum intensity projections of μ CT data sets (representative images of scores 4-1 are shown at bottom of table).

Description	Score
<i>Extent of Bony Bridging Histological Scoring Guide</i>	
Bony bridging entire span of the defect at longest point (8mm)	4
Bony bridging over partial length of the defect	3
Bony bridging only at the defect borders	2
Few bony spicules dispersed through defect	1
	0

Author Manuscript

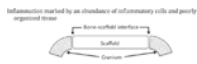
Author Manuscript

Author Manuscript

Author Manuscript

Table 3

Histological scoring guide for the extent of bony bridging, the extent of polymer degradation, and the tissue response at the bone-scaffold interface using longitudinal center-cut histological sections (diagram shown at bottom of table).

Description	Score
<i>Extent of Bony Bridging Histological Scoring Guide</i>	
Complete bridging	4
Greater than 70% bridged	3
40-70% bridged	2
10-40% bridged	1
Less than 10% bridged	0
<i>Scaffold Degradation Histological Scoring Guide</i>	
Decrease in hydrogel area	3
Excessive fragmentation (throughout hydrogel)	2
Minimal fragmentation (only at edges or outer surface)	1
Intact hydrogel	0
<i>Tissue Response at Bone-Scaffold Interface Histological Scoring Guide</i>	
Direct bone-to-implant contact without soft interlayer	4
Remodeling lacunae with osteoblasts and/or osteoclasts at surface	3
Majority of implant is surrounded by fibrous tissue capsule	2
Unorganized fibrous tissue (majority of tissue is not arranged as capsule)	1
	0

Author Manuscript

Author Manuscript

Author Manuscript

Author Manuscript